Prototype of Virtual Full Duplex via Rapid On-Off-Division Duplex

Zhen Tong[1], Christina Russ[2], Sundaram Vanka[3] and Martin Haenggi[1]

Abstract

We design and implement a software-radio system for rapid on-off-division duplex (RODD), a scheme to achieve virtual full-duplex communication at the level of a transmission frame. RODD is based on the insight that it is not necessary to separate a node's transmission and reception at the timescale of a frame. Instead, RODD allows each node in a network to follow a different random on-off signaling signature to transmit during its own on-slots and listen to its neighbors through its own off-slots. Over one frame interval, each node broadcasts its message to its neighbors while recovering its neighbors' messages from the superposed signals received via its own off-slots. In this paper, we describe an RODD prototype to prove its key concepts, including re-designed synchronization and coding schemes. Simulation results are presented for comparison with the measurements obtained from a software-defined radio implementation of RODD. The effects of on-off signaling on the performance are investigated experimentally. In particular, the bit error rate is measured and compared with the simulation results. Our results indicate that virtual full duplex is feasible on a USRPs/LabVIEW platform via RODD.

Index Terms

Full Duplex, Rapid On-Off-Division Duplex, Software-Defined Radio, Universal Software Radio Peripheral

[1]Zhen Tong (✉) and Martin Haenggi are with the Department of Electrical Engineering, University of Notre Dame, Notre Dame, IN 46556, USA, E-mail: {ztong1,mhaenggi}@nd.edu.

[2]Christina Russ is with Infineon Technologies.

[3]Sundaram Vanka is with Broadcom Corporation.

The partial support of the U.S. NSF (grant ECCS-1231806) is gratefully acknowledged.

I. Introduction

A. Motivation

Almost all radios used in commercial and military wireless networks currently are *half-duplex (HD)*. Due to the limited dynamic range of affordable radio frequency (RF) circuits, radios cannot resolve the desired signal picked up by their receive antenna when they are overwhelmed by their own transmitted signal. A node's own transmission picked up by its own antenna is typically many orders of magnitude stronger than the desired received signal (the power ratio can be anywhere from 15 dB to 100 dB [1]). This paper challenges the conventional wisdom of separating transmit and receive frames in time or frequency. We explore a novel *full-duplex (FD)* paradigm for the physical (PHY) layer of wireless networks based on *rapid on-off-division duplex (RODD)* [2]–[4].

The idea behind the RODD scheme is to let nodes follow an *on-off signaling signature*[1] to transmit over a sequence of slots, so that the node can receive a useful signal during each off slot. A slot spans one or several symbols. Therefore, the duration of one slot is hundreds of nanoseconds to a few microseconds. Using RODD signaling, all nodes in a network can transmit and receive simultaneously over every frame interval through their respective on-off signatures, hence achieving FD at the frame level, or *virtual* FD. Therefore, RODD enables half-duplex radios to achieve virtual FD communication.

While the theoretical results in the literature motivate the use of RODD, it is unclear if RODD is suitable in reality due to practical issues, such as hardware non-idealities and power leakage or strong inter-symbol interference from on-slot to off-slot caused by fast switching the signal on and off. It is also challenging to implement RODD in networks with asynchronous node behavior where nodes may become active at random times, and there is non-trivial overhead involved in detecting the frame(s) of interest in the presence of background noise and interference. These issues motivate the experimental study of RODD.

The goal of this paper is to prove the key concepts of RODD by implementing a prototype using software-defined radios and evaluating its performance. Using a combination of theory, simulation and experiments, it is shown that virtual FD can be achieved via RODD in a real wireless communication system. We also address practical implementation issues in the following sections.

[1]An on-off signaling signature is a randomly generated binary sequence.

Since the on-off RODD signal is not continuous as the signal in traditional communication systems, it poses challenges for physical layer design. Therefore, some signal processing blocks are re-designed specially for RODD, in particular the synchronization algorithm and the channel coding scheme.

B. Main Contributions

The main contributions of this work are summarized as follows:

- We propose a simple architecture to realize a practical RODD system with two nodes.
- We implement this architecture on USRP/LabVIEW [5] and determine the bit error rate (BER).
- We design a synchronization algorithm and channel coding scheme tailored for RODD and characterize the performance.
- On this prototype, we focus on the practical issues that arise in implementing RODD. In particular, we study the transient phase of the RODD signal and investigate and calibrate the effects that on-off signaling has on the system performance.

C. Organization

The remainder of the paper is organized as follows. In Section II, we briefly summarize the fundamental idea behind RODD, its advantage over the other FD techniques, and its applications. Section III describes the system architecture proposed to implement RODD while the synchronization and coding scheme are described in detail in Sections IV and V. We present the simulation and experimental setup of a single-link RODD system in Sections VI and VII. The BER curves are given and discussed together with the transients due to on-off signaling. In Section VIII, we conclude the paper and suggest directions for future work.

II. RODD Theory and Applications

A. RODD for Full Duplex

State-of-the-art MAC designs either schedule nodes orthogonally or apply a random access scheme. Random access may lead to poor efficiency while scheduling may be difficult and prone to overhead. RODD challenges the conventional paradigm of separating transmit and receive frames in time or frequency. The idea of RODD is to introduce off-slots in time within a frame

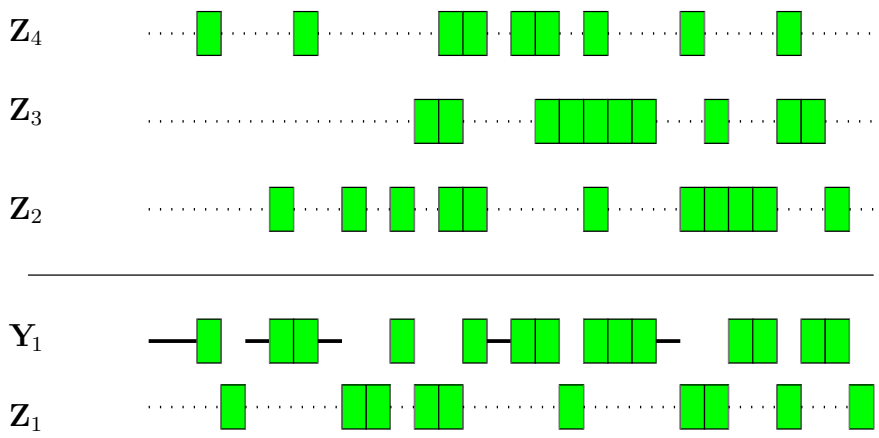

Figure 1: RODD signaling. $\mathbf{Z}_1, \mathbf{Z}_2, \mathbf{Z}_3, \mathbf{Z}_4$ represent the transmitted signals of node 1 through node 4, respectively, where the dotted lines represent off-slots and rectangles represent on-slots. The received signal of node 1 through its own off-slots is $\mathbf{Y}_1$, which is the superposition of $\mathbf{Z}_2$, $\mathbf{Z}_3$, and $\mathbf{Z}_4$ with erasures (blanks) at the on-slots of node 1.

of transmission through which the receiver can collect useful signals without contamination by self-interference. This allows a frame to be received (albeit with erasures) simultaneously as another frame is being transmitted. The received frame with erasures caused by self-interference can be recovered by channel coding specially designed for RODD, and there is no need for self-interference cancellation for either on-slots or off-slots. Hence, RODD enables half-duplex radios to achieve virtual FD communication and makes the radios appear as FD-capable to the higher layers although they are still half-duplex at the physical layer [3].

On-off keying is a decades-old technology [6], [7]. The sub-nanosecond response time of RF circuits allows fast switching (e.g., in time-hopping impulse radios [8]), at least in principle. Fig. 1 illustrates RODD signals over 30 slots in a frame, where symbol-level synchronous transmission is assumed for simplicity. If no node transmits in a slot then node 1 receives a zero signal represented by a solid line. Over the period of a single RODD frame, every node can broadcast a message to its neighbors, receive a signal, and decode the messages from its neighbors at the same time. Crucial to RODD is error-control coding over a frame of many on- and off-slots, which allows successful decoding despite erasures and superposition. In the multi-user case, a node's interference comes from its own transmitter and other transmitters as well while in the two-user case, only self-interference needs to be worried.

B. Advantages of Full Duplex via RODD

The standard FD technique is to let the receive chain of a node remove the self-interference caused by the known signal from its transmit chain, so that reception can be concurrent with transmission. The idea is not new (see, e.g., [9], [10]), but has only been successfully implemented in the industrial, scientific and medical (ISM) radio bands in laboratory environments in the past few years [1], [11]–[14]. Key to the success are novel analog and digital self-interference cancellation techniques (such as negating a wideband signal using a balanced/unbalanced transformer) as well as spatially separated (symmetric) transmit and receive antennas. We refer to this set of techniques as interference-cancellation-based FD (IC-FD), and IC-FD and virtual FD techniques are collectively referred to as FD techniques.

Each technique has its merit and weaknesses. RODD has to introduce off-slots in a frame in order to receive (which results in *virtual FD*), thus IC-FD may be more efficient if the self-interference can be perfectly removed in a single link. However, both transmitters in a link are always active in IC-FD, so there is more interference to the network [15], [16]. Even worse, some IC-FD schemes cancel self-interference by transmitting another signal opposite in phase for cancellation causing even more interference to the other nodes. Moreover, analog cancellation with multiple transmit antennas needs specially structured and symmetric antenna placement [17]–[19], because it is hard to reconstruct several self-interference signals accurately from their mixture for cancellation.

Compared to these schemes, RODD is "interference-friendly" due to the silent slots and hence may be a more viable solution. Self-interference caused by the on-slots leads to erasures at known locations. It is not necessary to perform self-interference cancellation for RODD, which can be complicated in both hardware and software. The same constraint of limited dynamic range of ADC still holds for RODD, and the RF circuits cannot resolve the desired signal picked up by its receive antenna when it is overwhelmed by its own transmitted signal. However, self-interference caused by power leakage or inter-symbol interference (ISI) from on-slots to off-slots needs only to be suppressed to some extent such that the desired signal during the off-slots can be resolved. This goal can be achieved even if the self-interference after suppression is larger than the desired signal as shown in Fig. 2. Hence, the requirement for self-interference suppression is far less stringent than self-interference cancellation for IC-FD. The power leakage or ISI may affect the

first few symbols during the off-slots. With carefully chosen pulse shaping filter, this issue can be resolved as we will show in the transient phase study in the experimental part.

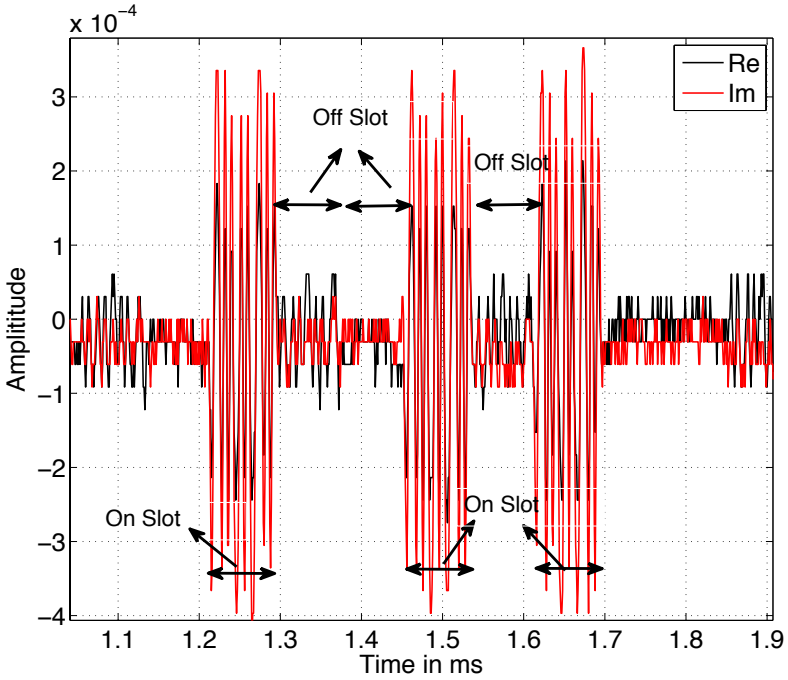

Figure 2: Baseband signal received at a USRP node while transmitting a DBPSK signal. The carrier frequency is 915 MHz. The transmit power is set to 0 during the off-slots, so that the device can receive a DBPSK signal from another transmitter. The DBPSK bits can be detected robustly even if the dynamic range between the two signals is large. The signal during the on-slots is the self-interference after suppression. The received signal during the off-slots would not be detectable in the digital domain if there was no self-interference suppression since the dynamic range of ADC is limited.

C. Applications of Full Duplex via RODD

Apart from potentially doubling the throughput of a link, there are many applications for RODD: one such application is continuously cognitive radios [20]. The question of when to transmit and when to sense the channel has commanded much research effort in the area of cognitive radios. The premise that a radio cannot be cognitive during transmission, however, shall be revised if the secondary users use RODD. A virtual FD radio stays cognitive continuously, ready to abort transmissions as soon as any primary radio is sensed during its off-slots. This dramatically reduces disruption to primary users.

Many advanced network protocols require knowledge of the state of communicating parties, such as the power, modulation format, code rate, ACK, queue length, etc. Such *network state information (NSI)* is typically intended for multiple neighbors, of fewer bits than application data, and more sensitive to delay. NSI is conventionally treated similarly as data and thus subject to contentions. As a result, the overhead of exchanging NSI often dominates the data traffic in a mobile network. RODD is ideal for NSI exchange: a frame can be reserved, in which all nodes simultaneously broadcast local NSI to their respective neighbors; each node then decodes the NSI from all neighbors at once. In fact, a new sub-layer of the protocol stack devoted to NSI can be designed based on RODD techniques. Other applications include Carrier-sensing Multiple Access (CSMA) with collision detection and instantaneous feedback (and ACK/NACK) using RODD.

III. Implementing an RODD system

The RODD system described in [2]–[4] is an ideal system with Gaussian channels and perfect synchronization. However, in a practical system, imperfect synchronization negatively affects the system performance. To implement RODD, there are several critical practical issues that need to be solved. The detailed choice and setup of the platform will be discussed in Subsection III-A.

Subsection III-B will introduce the frame structure that is tailored for an RODD system. The overall implementation of our RODD system will be described in detail in Subsection III-C, which also covers the differences from traditional communication systems.

A. Platform

We implemented all physical layer processing for RODD by suitably modifying a novel point-to-point wireless testbed based on equipment from National Instruments (NI). The design parameters are specifically chosen based on the RODD properties. The testbed runs on NI LabVIEW on a Windows host computer. NI LabVIEW provides driver functions that interface the host computer with the NI USRP boards [5] that comprise the analog front end and the RF part.

As mentioned in Section II-B, the advantage of RODD over IC-FD is that for RODD, it needs only self-interference suppression instead of self-interference cancellation. We implement the self-interference suppression in two ways: one way is to use a two-antenna setup. For one

user, we use one antenna for the transmit RF chain to transmit on-off signals while a second antenna is used for the receive RF chain to receive the signals continuously. For example, a Tx-Rx antenna separation of about 15-20 cm results in a path loss of about 40 dB (depending on the channel characteristics). Hence, we can adjust the separation between the Tx and Rx antennas according to the link distance between the users. The two-antenna setup may appear cumbersome; an alternative is to use a circulator between the Tx and Rx paths to separate the transmitted and received signal. The isolation of the circulator is usually at least 15 dB with an insertion loss of 1 dB at most, which is acceptable for our application if the link distance is short. Larger separation can be achieved by designing a simple balanced feed network using two circulators and two hybrid power combiners as in [21]. It has been shown in [21] that this technique can provide over 40 dB isolation between the transmitter and receiver channels at only 0.75 dB insertion loss for the transmitter-to-antenna and antenna-to-receiver paths. In this paper, we present results obtained using both setups, the one with two antennas and the other with one antenna and one circulator and demonstrate that both work very well. Fig. 3 shows the two different setups for self-interference suppression. The baseband signal at one USRP node while transmitting a DBPSK signal based on the two-antenna setup is illustrated in Fig. 2.

(a) Hardware setup with two antennas (b) Hardware setup with one antenna and circulator

Figure 3: Two different hardware setups for self-interference suppression.

The two-antenna setup is illustrated in Fig. 4b. Each USRP is equipped with two antennas,

one to transmit and one to receive. The setup includes a line of sight (LOS) between Tx1 of USRP #1 and Rx2 of USRP #2 and between Tx2 of USRP #2 and Rx1 of USRP #1; the LOS paths are partially shadowed by the other antenna of each USRP. We evaluate the received signal at both Rx1 and Rx2 of two USRPs for our performance measurements. USRP #2 is connected via Ethernet cable to the host, which enables the programming of the USRPs via NI LabVIEW. The setup has two modes: the unidirectional setup is used as benchmark for the RODD system where only one Tx-Rx path is used via cable connection, i.e., the Tx2 of USRP #2 is connected to Rx1 of USRP #1 via an RF cable with attenuators as shown in Fig. 4a; the bidirectional mode is our normal RODD setup with antennas and transmission over the air as shown in Fig. 4b. The MIMO cable is used here for clock sharing between these two USRPs such that they can be controlled to transmit and receive at the same time. The attenuators are used between the RF front end and the transmitter and receiver antennas to make the testbed operate at different signal-to-noise ratios (SNRs). Attenuators are used because even if the transmit power gain is set to the minimal value of 0 dB, the SNR is still too high due to the proximity of the two USRPs. The setup with one antenna and one circulator is illustrated in Fig. 4c where USRP #1 uses one circulator to provide at least 19 dB [22] separation between the transmit and receive signal while USRP #2 still uses the two-antenna setup as a reference.

B. Frame Structure

Conventionally, transmissions occur in frames with continuous signals. However, a frame in an RODD system is divided into many slots as discussed earlier, and thus a special frame structure is needed. Similarly to IEEE 802.11, the frame consists of a preamble followed by a payload. The preamble consists of P identical training sequences (this is equivalent to the short training sequences in the WLAN preamble [23]), each training sequence comprising L symbols, which is specifically designed to be the same as the number of symbols in an RODD slot. By doing so, each training sequence will be assigned to exactly one on-slot during the transmission. The length of the payload M is chosen to be a multiple of the slot length L; otherwise zero padding at the end of the payload is needed. The repeated training sequences are also very helpful to the timing estimation at the receiver as discussed in detail in Section IV. The RODD frame structure is depicted in Fig. 5. Further, since the timing does not change significantly over one frame, it is sufficient to estimate the symbol timing once at the beginning of each frame.

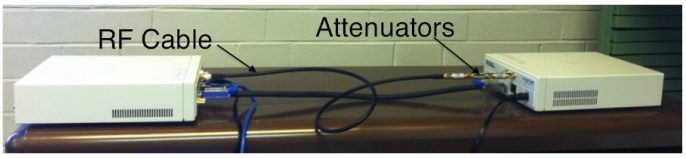

(a) Unidirectional setup

(b) Bidirectional setup with two antennas

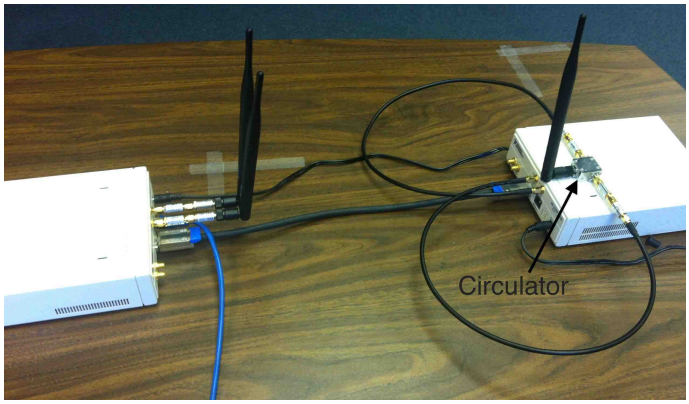

(c) Bidirectional setup with one antenna and one circulator

Figure 4: Setup of two NI USRPs connected via MIMO cable to each other for unidirectional and bidirectional experiments. The unidirectional setup is used to exclude the effects of self-interference, multipath propagation, and other channel impairments and serves as a benchmark for comparison with the bidirectional setup.

C. Transceiver Chain

The basic elements of the RODD transceiver chain are shown in Fig. 6. Between the Pulse Shaping Filter block and the channel, there are the upconverter and other RF front end components which are part of the USRPs and therefore omitted in the block diagram. Similarly, between the channel and matched filter block, the signal is received by the antenna and downconverted by the USRPs. The baseband signal is fed into the Matched Filter block for processing. For this prototype we assume that each node knows the on-off signaling signature of the other node

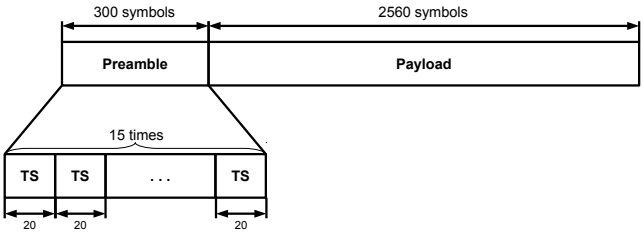

Figure 5: RODD frame structure where $P = 15$, $L = 20$, and $M = 2560$. TS is short for training sequence.

besides its own signature. This is also the assumption in [2]–[4]. One of the advantages of using random on-off signaling is that there is no need to coordinate different nodes to transmit in order to avoid collisions. One may argue that it is preferable to avoid collisions by using a fast TDMA scheme, at least for the two-node case. However, it is beneficial to use random on-off signaling for the multi-user case where the coordination to avoid collisions is more difficult. The two-node RODD prototype serves as a proof-of-concept and building block for the multi-user case.

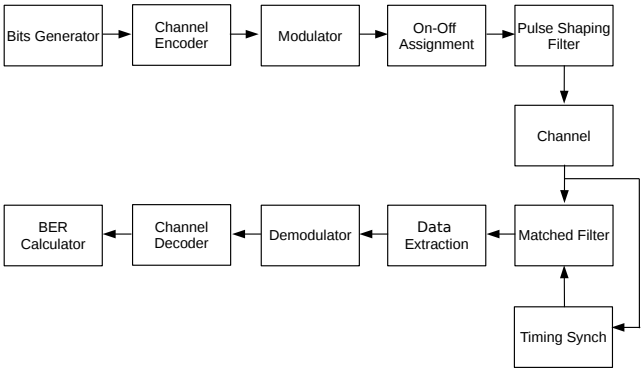

Figure 6: Block diagram of the RODD transceiver chain.

1) Transmitter Operation: A source bit stream is first generated randomly. Another random sequence whose length equals the slot length is also generated in a similar way to serve as the training sequence in the preamble and is assumed to be known to all nodes in the system. The data payload is encoded by the channel encoder and concatenated with the preamble. The channel code is a specially designed concatenated code whose implementation is discussed in Section V. Then the frame that consists of preamble and payload enters the modulator. The

option DBPSK is used in our prototype since it is more robust to the phase offset introduced by hardware.

To assign the slots in one RODD frame, an on-off signature is generated in a random fashion. Each node has an unique signature, which is a binary sequence. Once randomly generated, a node's signature remains the same for each frame afterwards. The signature is split into equally sized segments of length $\left[\frac{1}{\text{duty cycle}}\right]$, where the duty cycle is the fraction of ones in the on-off signature and $[\cdot]$ denotes rounding to the nearest integer. It may lead to insufficient on-slots if we take a purely random on-off signature with the desired length instead of the signature grouped into equally-sized segments. If the duty cycle is, e.g., $1/3$, the size of one segment is 3. Within one segment, one slot is assigned randomly as on-slot while the others are assigned as off-slots. A frame after on-off assignment is called an on-off frame. The on-off frame size is calculated as the product of the number of bits per frame and the inverse duty cycle. With a duty cycle of $1/3$, 2560 bits in payload and 15 20-bit training sequences, the on-off frame size is calculated as follows:

$$\text{on-off frame size} = (2560 + 15 \times 20)/(1/3) = 8580.$$

After the signature is generated, the data is assigned to the specified on-slots in an on-off frame. Whenever the signature is one, a slot of the modulated signal is passed to the output; otherwise, an array, containing only zeros, with size of one RODD slot, is passed to the output. Here, "zeros" means the transmitter is "sending" a null signal to allow reception from other nodes.

A pulse shaping filter is used to change the waveform of the transmitted pulses in the same way as in a conventional communication systems. The pulse shaping filter is the commonly used root raised cosine filter with rolloff factor 0.5. Although the introduction of zero symbols in the off-slots will expand the bandwidth of the RODD signal, the pulse shaping filter will truncate it in the frequency domain to prevent energy leakage outside the bandwidth of the filter. Band limiting the signal causes power leakage from the on-slot into the off-slot in the time domain at the receiver side. We will discuss and calibrate this leakage in Section VII-B. At the end of the transmit chain, the generated baseband signal is sent to the USRP for transmission.

2) Receiver Operation: First the receiver needs to detect the starting point of the frame. An energy detector is used for frame detection while a crosscorrelation-based timing estimation algorithm is designed to find the precise symbol timing information. A matched filter with

parameters corresponding to the pulse shaping filter at the transmitter side is applied to the received signal followed by a decimator.

Following the decimator is the data extraction block for the non-erased on-slots. The resulting signal is a truncated version of the received signal, starting at the first training sequence that has been received successfully. The preamble is used for synchronization as discussed in the following section. The actual starting point of the data is calculated using the information about the number of received preambles without erasures, which is provided by the synchronization block. The output array of the extraction block contains only the received data during the receiver's off slots without the erased data. The incoming symbols are demodulated in a hard-decision fashion to the corresponding output bits. Then the demodulated bits are sent to the channel decoder that will try to recover the erased slots based on the received data. In the end, the recovered bits will be fed into the BER calculation block to obtain the BER by comparing them to the transmitted bits.

IV. Synchronization for RODD

There are two levels of synchronization. The first level of synchronization is that of different users. The way to synchronize different users is to let them share a common clock. For example, a MIMO cable may be used for the two-user case. As a result, different nodes can transmit and receive at the same time. Such synchronization is not mandatory for an RODD system, as discussed in [2], but it simplifies the implementation. Although the MIMO cable synchronizes the clock of two USPRs, there is still a small frequency offset due to hardware non-idealities.

The second level of synchronization includes the timing estimation, frequency synchronization, and channel estimation. What makes the synchronization more challenging in the RODD system than in a conventional communication system is that the received signal is an on-off signal with erasures. Hence the need to design an RODD-specific synchronization algorithm. Similar to a traditional communication system, a known training sequence is needed. To avoid a packet drop due to a failed reception of the training sequence, we need to guarantee that the training sequence is received without erasure. Therefore, we adapt the preamble structure in the IEEE 802.11 standards and add it at the start of the packet as shown in Fig. 5. To increase the likelihood that at least one training sequence in the preamble is received without an erasure due to self-interference, we send the same training sequence P times in the preamble. Thus the probability

that all training sequences collide with a node's self-interference is $(\text{duty cycle})^P$. For a duty cycle of $1/3$ and $P = 15$, this probability is 7.0×10^{-8}, which is negligible given that our simulation runs are only 10000. In general, the number of repeated training sequences P and hence the length of the preamble should increase as the duty cycle increases.

Another feature that is specially designed for RODD is that the length of a training sequence is the same as the slot length, as discussed earlier, with the advantage that the training sequence will be assigned to exactly one on-slot, which is easy to implement. Those received training sequences in the preamble without erasure can then be used for timing estimation, frequency synchronization, and channel estimation. In the following, we mainly focus on the design of the timing estimation algorithm since the absence of frequency synchronization and channel estimation has a small impact on the performance due to the choice of differential binary modulation and the narrow bandwidth of the system.

Even in the synchronized case where the nodes start to transmit and receive at the same time, the receivers do not know exactly when a packet starts since there is latency introduced by the data transmission from the host to the radios and back. Therefore, detecting the packets is the very first step of the successful reception and obviously of central importance for good performance.

Usually, the timing estimation consists of two main tasks: packet detection and symbol synchronization. Packet detection is the task of finding an estimate of the start of the preamble of an incoming data packet. In our design, an energy detector [23] is used for packet detection for its simplicity. The energy is estimated by calculating the energy of a sliding window. The length of the sliding window is chosen to be one slot size L. If the accumulated received signal energy exceeds a certain threshold, the detector forwards the truncated signal to the next stage for symbol synchronization.

Symbol synchronization is the task of finding the precise moment of when the first symbol starts. It is achieved using a modified crosscorrelation-based timing estimation algorithm [23] since the receiver has the knowledge of the preamble, i.e., the repeated training sequences. The block diagram of the algorithm is illustrated in Fig. 7. In the sliding window C, the incoming signal r_n is cross-correlated with the known training sequence t_k, which is a pseudo-random sequence. P_1 and P_2 calculate the square root of the accumulated energy for r_n and t_k over a window of slot length, respectively.

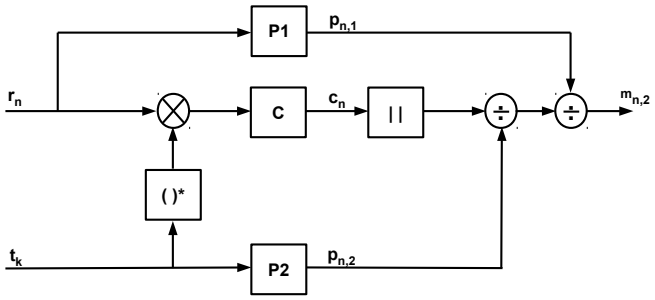

Figure 7: Flow graph of symbol timing estimation algorithm in the RODD system where r_n is the incoming signal and t_k is the training sequence.

The decision statistic $m_{n,2}$ is

$$m_{n,2} = \frac{|c_n|}{p_{n,1}p_{n,2}}, \tag{1}$$

where c_n is the crosscorrelation between the known training sequence and the incoming signal over a sliding window with length L and $p_{n,1}$ and $p_{n,2}$ are the square roots of the accumulated energy of the signals r_k and t_k over a sliding window with length L. Since $m_{n,2} \in [0, 1]$, it does not depend on the absolute energy level.

Finally, when the correlator output exceeds a certain threshold, which needs some fine-tuning in the simulation and experiments, it provides a coarse starting point n_s. The maximum of the next N calculated decision statistics (starting at n_s) is taken as the estimated starting point of the preamble:

$$\hat{n}_{\text{start}} = \arg\max_{n} |m_{n,2}|, \tag{2}$$

where $n \in \{n_s, n_s + 1, \ldots, n_s + N\}$. The choice of N is discussed in the appendix.

As an example, the simulation resulting output $m_{n,2}$ of the synchronization is presented in Fig. 8. The plot shows 9 peaks that are significantly higher than the rest of the output and above the threshold. Those peaks are the remaining 9 training sequences out of $P = 15$, which are not erased by the node's self-interference. The algorithm needs at least one remaining training sequence to work quite accurately. The other peaks could be used to improve accuracy or for other purposes such as frequency estimation and channel estimation.

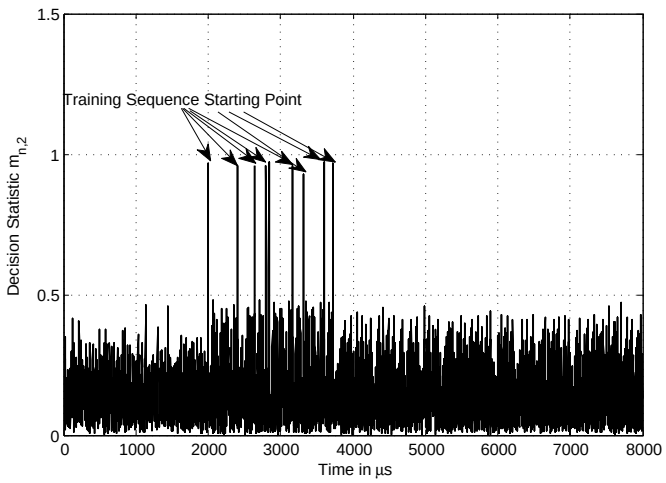

Figure 8: Simulation output $m_{n,2}$ of symbol timing estimation algorithm using RODD signaling with duty cycle $1/3$, $P = 15$ and SNR $= 15\,$dB.

V. Channel Coding for RODD

The RODD channel is a combination of an erasure channel and an AWGN channel. Both Cauchy Reed Solomon (Cauchy RS) codes and Vandermonde Reed Solomon (Vandermonde RS) codes are good codes for erasure channels. Theoretically, RS codes can detect and correct combinations of errors and erasures. In the following, we propose a concatenated code with a Vandermonde RS code as outer code and a variation of a parity check as inner code to serve as the channel coding scheme in the RODD system to recover the message in presence of erasures and Gaussian noise errors.

A. Code Design

The erasures in the RODD channel are caused by self-interference at known positions to the receivers and errors are caused due to Gaussian noise. To correct both errors and erasures, we use an inner code to detect noise errors for each non-erased on-slot and label it as an erasure and a Vandermonde RS code as an outer code to correct the erasures.

1) Inner Code: The inner code uses a parity bit at the end of each on-slot to detect the noise errors if there is no erasure from self-interference. Given the slot length L, the first bit of an on-slot is not used and serves as a guard bit since it does not convey any useful information due to the choice of DBPSK. The information of a DBPSK symbol is encoded in the relative

phase shift. Consequently, since the continuous signal is cut into pieces (slots), the information for the first symbol in an on slot may get lost if its previous slot gets erased. The last bit of an on-slot is preserved as a parity bit. Since DBPSK is used, the errors tend to come in pairs. Therefore, the parity bit is chosen as the modulo-two-sum of the bits in the even-numbered-positions, i.e., the parity bit is $x_{k,L} = \left(\sum_{i=1}^{L/2-1} x_{k,2i}\right) \mod 2$, where the k^{th} on-slot consists of $[x_{k,0}, x_{k,1}, x_{k,2}, \cdots, x_{k,L-1}, x_{k,L}]$. Any two-bits-adjacent error event will affect exactly one bit in an even-numbered position and thus will be detected by a violation of the parity. Such a code can detect one error event in an on-slot. This is enough for our application since the slot length L is short.

2) Outer Code: The outer code is an off-the-shelf Vandermonde RS code for erasures correction. In the following, we will discuss the parameters for the outer code.

1) *Size of Data Symbol*

The size of a data symbol in an RS code decides whether the RS code can be implemented efficiently, i.e., if the RS decoder is too slow and there may be overflow since the incoming signal will be accumulated in the decoder. Since the RS codes are implemented in Galois field GF$[2^s]$, where s is the number of bits in one data symbol, a large s will incur significant computational effort. A natural choice is to choose $s = L - 2$, where L is the slot length in bits in the RODD signal. In our experiment, $L = 20$, which would make s too large. Normally, the value of s lies between 2 and 16 for efficient computation. Given the slot length $L = 20$, the size of data symbol in our RS code is chosen to be $s = 6$. As a result, there are $S = 3$ data symbols in one on-slot plus the first bit and last bit, i.e., $S \times s + 2 = L$. For different slot lengths L, the data symbol size s can be varied as long as $L - 2$ is a multiple of s.

2) *Code Rate*

For the one-link experiment with duty cycle $1/3$ for the on-off signature, the channel erasure rate is $1/3$. Since the erasure positions are known to the receiver, $n - k \geq \frac{1}{3}n$ leads to $\frac{k}{n} \leq \frac{2}{3}$. It means that the code rate can be at most $2/3$ in this case without considering Gaussian noise. Theoretically, we can choose an RS code with code rate $2/3$ for an RODD signal with duty cycle $1/3$ to correct one erasure out of 3 slots on average. Therefore, the throughput can be up to $\frac{1}{3} \times \frac{2}{3} = \frac{2}{9}$ for a two-user RODD system, which is the same as that of a two-user slotted ALOHA system with transmit probability $1/3$.

However, the instantaneous erasure rate is a random variable with the duty cycle as its average. As a result, it is sensible to use a lower code rate or a variable-rate code that is based on the number of actual erasures in each frame. Here, we choose a Vandermonde RS code (n, k) as $(64, 32)$ with code rate $1/2$ to provide some resilience for the RS code. The erasure rate can be higher than $1/2$ with small probability, in which case the RS code cannot decode the message correctly. For a (n, k) RS code, the probability that the erasure rate is higher than $1 - k/n$ is

$$\begin{aligned}\mathbb{P}\left(\left\{\text{erasure rate} > 1 - \frac{k}{n}\right\}\right) &= \mathbb{P}\left(\{\text{more than } n-k \text{ slots erased}\}\right) \\ &= \sum_{i=n-k+1}^{n} \left(\frac{1}{3}\right)^{i} \left(\frac{2}{3}\right)^{n-i},\end{aligned}$$

which is 0.2% for RS $(64, 32)$. Although 0.2% is small, it will limit the coding performance if no special care is taken. Hence, in our implementation, we choose the two random on-off signatures such that the erasures caused to each other will not exceed $n - k$ out of n. We also analyzed the tradeoff between code rate and the duty cycle in the appendix.

3) *Noise Errors*

The Vandermonde RS code is designed based on the assumption that the erasure locations are known. The erasures are caused by self-interference, and their locations can be derived from the on-off signatures. However, the locations of the noise errors are unknown. Detecting noise errors is the purpose of the parity bit. It reveals if an on-slot has an error event or not. If it does, this slot is labeled as an erasure and its location is known then. In the end, we only use the on-slots that have no erasures or noise errors to recover the message. By doing so, the coding performance will be improved. For the high-SNR regime, the number of noise errors is small, and the inner code is sufficient to flag all erasures caused by the noise errors. For the low-SNR regime, it is possible that many non-erased on-slots are contaminated by noise errors and hence the decoder is forced to use some of them together with the non-erased on-slots without noise errors to decode.

4) *Other Parameters*

For an uncoded frame of length 1280 bits, there are 64 on-slots. We divide them equally into two parts and each is encoded by RS $(64, 32)$. As a result, the encoded frame length will be doubled, i.e., 2560 bits. More details about the implementation of the Vandermonde

RS code can be found in [24], [25].

B. Discussion

The inner code detects the error and labels the slot as an erasure if there is one error event. There are ways to improve its performance. For example, an alternative code is obtained by using a different RS encoder/decoder that can correct both erasures and errors instead of a Vandermonde RS code that only correct erasures. The advantage is that the redundancy in the RS code can be fully exploited. On the other hand, the Vandermonde RS code has the advantage that the decoder can start decoding once the receiver obtains enough correct data symbols, i.e., k non-erased on-slots in RODD frame for an RS (n, k) code, which reduces the latency.

The choice of channel code is application-specific depending on the delay constraint and other system requirements. Fountain codes [26] (also known as rateless erasure codes) are a class of erasure codes with the property that a potentially infinite sequence of encoding symbols can be generated from a given set of source symbols such that the original source symbols can ideally be recovered from any subset of the encoding symbols of size equal to or only slightly larger than the number of source symbols. These codes may be particularly suitable if we apply RODD to a feedback system, in which the receiver can send an ACK back to transmitter if it receives enough symbols to decode the message.

From a channel access perspective, RODD can be considered as a slot-level random access scheme. Its advantages over the popular MAC schemes have been discussed in [3] where the differences between RODD and CDMA, TDMA, ALOHA and CSMA are described in detail. We would like to emphasize that RODD is similar to slotted ALOHA but operates at a much faster timescale. Consequently, ALOHA cannot achieve the same throughput as RODD unless it encodes across frames in order to correct the frame erasures instead of slot erasures, which is impractical since, in that case, the receiver needs to wait for a long time (many frames) in order to decode the coded frames. This would make the decoding delay prohibitively long. On the other hand, the decoding delay of RODD is always at most one frame interval. In [27], [28], coded slotted ALOHA has been studied extensively by using packet erasure correcting coding and successive interference cancellation. Besides different time scales and hence significant decoding delay, coded slotted ALOHA assumes an erasure channel where the noises can be dealt with by physical layer coding perfectly while RODD has a channel that is a combination of noise and

erasures.

VI. Simulation Results

The purpose of the simulations is to verify the functionality of the RODD system over simulated AWGN channels. Each block in the system such as the SNR estimator, timing synchronization block, and channel coding block can be tested. In this section, simulation results and, in particular, BER versus energy per bit to noise power spectral density ratio (E_b/N_0) curves (in the following denoted as BER curves) of the RODD implementation are shown and discussed.

A. Simulation Setup

In the following we discuss the parameters that are used for the LabVIEW simulation. At the beginning of each frame we add 100 zeros to serve as guard bits between frames. The pseudo-random generated training sequence is repeated $P = 15$ times and randomly assigned to slots at the beginning of an on-off frame. DBPSK is chosen for the experiments as well as simulation for the following reasons: the real channel, in general, introduces an unknown phase-shift to the PSK signal; in these cases the differential schemes can yield a better error-rate than the coherent schemes. This is true even if two USRPs share the same clock. We decided to use binary modulation because the decision regions in the constellation graph are larger than for larger constellations, such as, QPSK or 8-PSK. The results are averaged over $10\,000$ runs. The transmit power level is set to 0 dBm for the simulation. The results are obtained for a simulated AWGN channel with path loss values from 61 dB to 70 dB for self-interference and from 76 dB to 85 dB for the link, respectively, while the noise level is fixed at -90 dBm. The parameters are summarized in Table I.

B. Simulation Results

The simulated BER curves are shown in Fig. 9. We observe a noticeable difference of the uncoded BER curves compared to the coded BER curve. It is mainly due to three factors: erasures, timing errors, and first-bit inaccuracy in the on-slots due to DBPSK. The erasures have significant effects on the BER even among the different uncoded BER curves. With a $1/3$ erasure rate, the uncoded BER curve with erasures has an error floor of around $\frac{1}{3} \times 50\%$, which is shown in Fig. 9. The coded curve shows that coding can deal with the erasures very well.

Parameter	Value
frame size M	2560 symbols
slot length L	20 symbols
N	5
duty cycle	$1/3$
number of repeated training sequences P	15
inner code	(19,18)
outer code	RS (64,32)
pulse shaping/matched filter	root raised cosine pulse
rolloff factor	0.5
filter length	6 symbols
oversampling factor	4
AGWN level	-90 dBm
sampling frequency	800 kHz
modulation type	DBPSK
simulated transmit power	0 dBm

Table I: Simulation Parameters

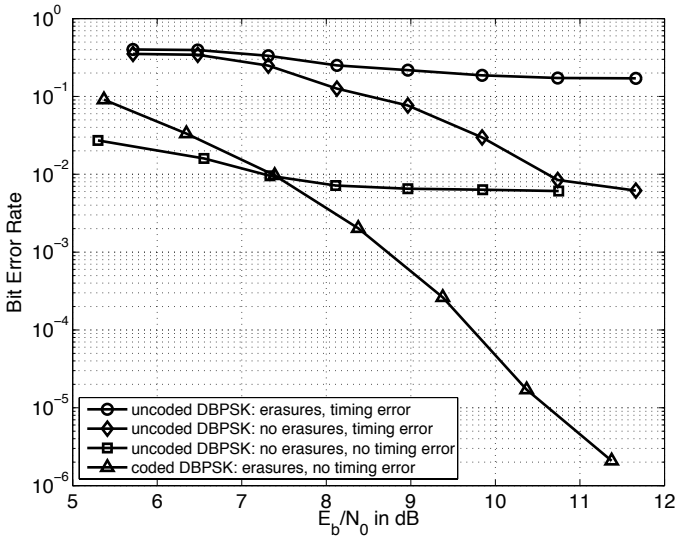

Figure 9: BER curves of RODD simulation.

Fig. 10 shows the timing estimation accuracy in the simulation. Timing estimation accuracy is defined as the ratio of the number of iterations with accurate timing estimation and the total number of iterations. In the low-SNR regime, the BER difference between the uncoded and coded case is mainly caused by the timing error. For example, at an SNR of 6 dB, the timing

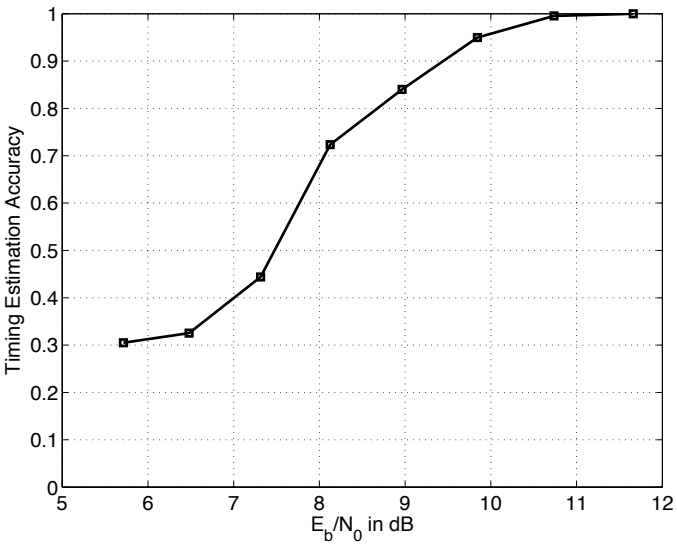

Figure 10: Timing estimation accuracy of RODD simulation.

error is about $1 - 0.3 = 0.7$ from Fig. 10. When the timing is wrong, the packet will have about 50% BER. Therefore, the BER is about $0.7 \times 50\% = 0.35$, in agreement with the value from Fig. 9. The timing errors can be fixed by boosting the preamble power by 3 dB in the low-SNR regime, i.e. by doubling the preamble power as in [29] to achieve nearly perfect synchronization.

In the high-SNR regime, i.e., SNR greater than 10 dB, there is an error floor in the uncoded BER curves without erasures. The first bit is error-prone due to the choice of DBPSK, as discussed in Section V. As a result, we ignore the first bit in a slot since it does not convey any useful information. Moreover, we will show in the following that the first bit may be distorted by the leakage from the previous slot if the previous slot is self-interference. Therefore, the first bit is reserved as a guard bit. The coded BER curve without timing errors is much better than the uncoded curves for the high-SNR regime where the timing accuracy is not an issue. Compared to the uncoded curves without timing error or erasures, the coded curve is better in the high-SNR regime and slightly worse in the low-SNR regime where the channel code can not correct all erasures due to the many noise errors.

VII. Experimental Results

A. Setup

For the measurements on the USRP platform most of the parameters are the same as for the simulation so that the results can be compared. Some parameters are changed or additionally needed in order to meet the hardware requirements. They are discussed in the following.

The system operates in the $915\,\text{MHz}$ ISM band with an IQ sampling rate of 800 kS/s. The starting time for the transmitter is set to $1.2\,\text{s}$ which is the same as that for the receiver. The reason is that the hardware initialization may take up to $1.2\,\text{s}$.

To measure the BER curve on the USRPs, we used two different implementations: the unidirectional mode and the bidirectional mode, as illustrated in Fig. 4. Comparing the two modes, we get an idea of how a node's own transmitted signal affects its receive performance. The settings for certain measured E_b/N_0 values are summarized in Tables II, III and IV in the appendix. For the unidirectional mode the setup illustrated in Fig. 4a is used. An RF cable is used for transmission between Tx1 of USRP #1 and Rx2 of USRP #2. The setups in Fig. 4b and Fig. 4c are used for the bidirectional mode, one with two antennas and the other with one antenna and one circulator. Hence, the bidirectional mode is additionally affected by fading or other channel impairments caused by the wireless channel and self-interference. The received signals at both receivers are evaluated. The two USRPs are connected via a MIMO cable. This connection enables the option to share the clock and is used to synchronize two users between the two USRPs as discussed earlier. Therefore the synchronization is more reliable over one frame. The second USRP uses the clock and the frequency reference of the first USRP. Note that due to hardware imperfections, there is still small a frequency offset between these two USRPs. The experiments are run to transmit $10\,000$ frames continuously to obtain the averaged BER values. We focus on the performance without timing errors in experiments.

B. Transient Analysis

The rapid switching in RODD signals leads to transients that may affect the performance. In this subsection, we study the impact of these transients by taking measurements from specifically designed experiments. In particular, the goal is to determine the number of symbols that can be potentially impaired by the transients. Fig. 11 shows a typical on-off signal with 20 DBPSK-

symbols per slot and a duty cycle of $1/3$. The oversampling factor is 32 instead of 4 in order to obtain a good resolution of the signal in the time domain.

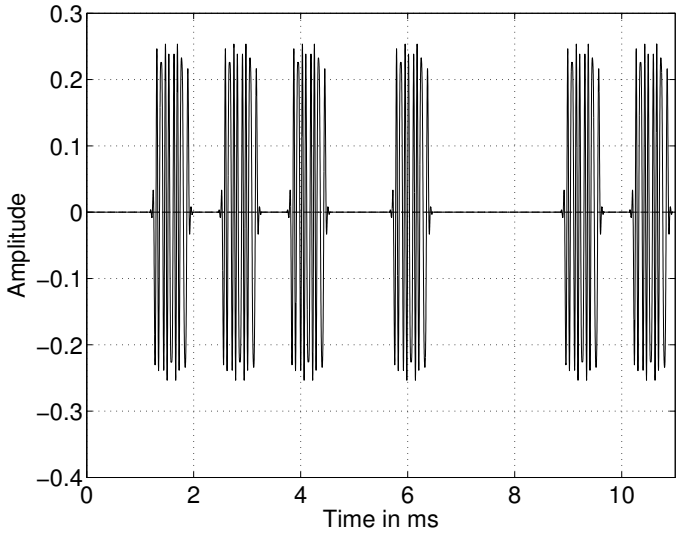

Figure 11: On-off signaling with 20 DBPSK symbols per RODD slot and duty cycle $1/3$.

The generated signal (DBPSK symbols) is separated into on- and off-slots of certain duration (here 20 symbols). The off-slot in this sense is a period of time during which the USRP does not transmit DBPSK symbols but only null symbols. The on-slot is the time period where the USRP transmits data.

First, we examine the time of one symbol and compare it with the duration of its side lobes. The theoretical duration of one symbol is

$$T_{symbol} = \frac{32}{800\,\text{kHz}} = 40\,\mu\text{s}. \tag{3}$$

As measuring only one symbol's duration is very inaccurate, we took the average over 20 DBPSK symbols, as shown in Fig. 12. The duration of the on-slot is measured without the side lobes. The starting and the end points are shown in Fig. 12 with vertical lines. The on-slot was measured to last $830\,\mu$s. Therefore the duration of one symbol is $41.5\,\mu$s and thus similar to the theoretical result.

Focusing on the transient phase between on- and off-slots, Fig. 13 shows the transient due to the switching from an on-slot to an off-slot (upper plot) and the other way around (lower plot). The duration of the significant side lobes is measured to be $80\,\mu$s, which is roughly two

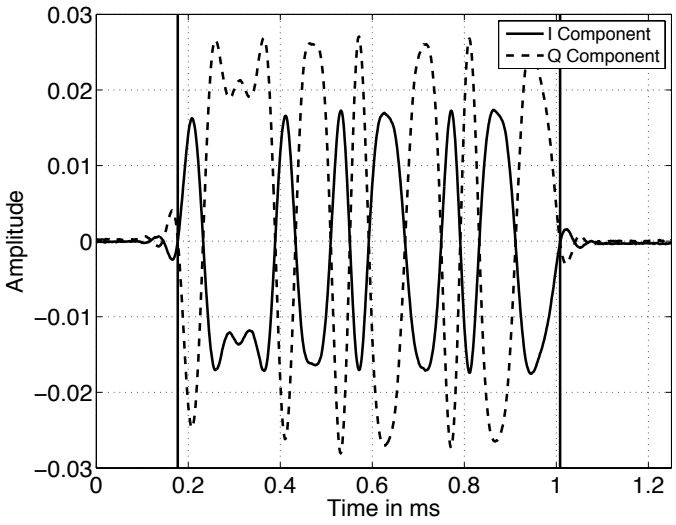

Figure 12: Plot of received RODD on-slot containing 20 DBPSK symbols with sampling rate 800 kHz and oversampling factor 32. The duration of the on-slot is measured to be 830 μs.

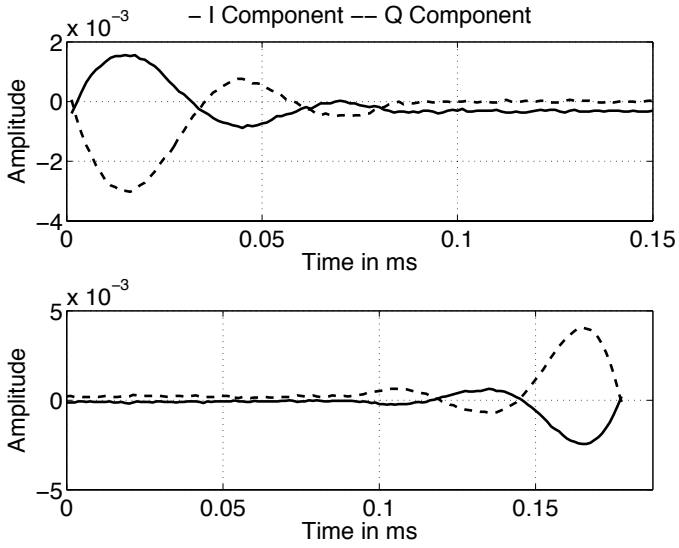

Figure 13: Transient between on- and off-slot (upper plot) and transient between off- and on-slot (lower plot) at Rx side.

symbol durations. Examining the side lobes we see that only the first side lobe has a significant amplitude. Thus, we conclude that most parts of the side lobes disappear within one symbol duration in relation to the measured symbol duration for chosen symbol rate.

To quantify the length of the transient, we examine the average received signal power during

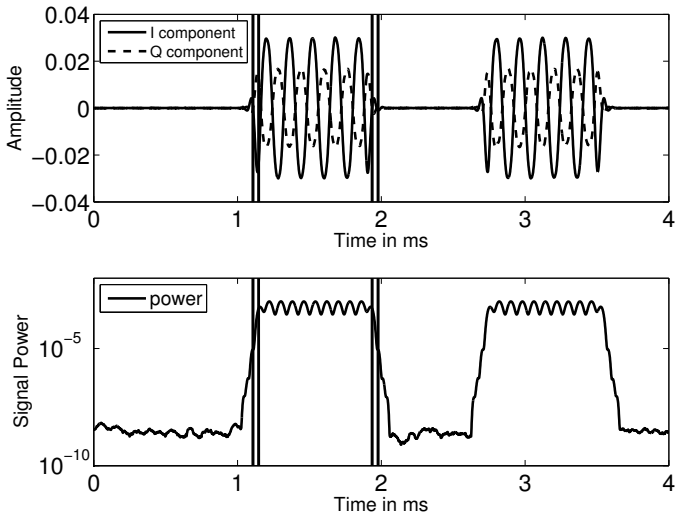

Figure 14: RODD signal containing two on-slots (upper plot) and estimated energy of the signal (lower plot).

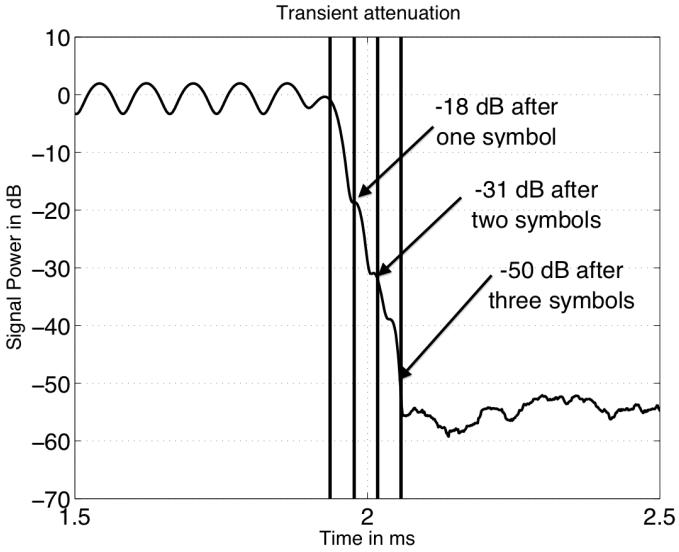

Figure 15: Received signal power gain at the transient from an on-slot to an off-slot. Markers are set in 32 samples distance to indicate the number of symbols after the on-slot.

and after an on-slot. A sequence of on- and off-slots is extracted from the whole signal and plotted in Fig. 14 (upper plot). The average power for the duration of one symbol (32 samples) is calculated with a sliding window of size 32:

$$\bar{P}_k = \frac{1}{32} \sum_{i=0}^{31} |r_{k+i}|^2 . \tag{4}$$

The resulting power figure is shown in Fig. 14 (lower plot). The first vertical line indicates the starting point of the on-slot. The fourth vertical line is exactly 32 samples after the on-slot, i.e., one symbol duration later. To calculate the average power $\bar{P}_{on}$ over one on-slot, values starting at the second vertical line and ending at the third vertical line are used. The second vertical line is exactly 32 samples after the on-slot started. Thus the moving window is fully covered by the on-slot at this time. The third vertical line is exactly at the end of the on-slot. We use the average power over this interval as a reference to calculate the attenuation of the following signal compared to the on-slot. To do so, we divide the estimated average power values by this value and convert the result into dB:

$$\text{gain}^{(\text{dB})} = 10 \log_{10} \left(\frac{\bar{P}_k}{\bar{P}_{on}} \right). \tag{5}$$

The trend of the signal power gain is illustrated in Fig. 15. The average power after one symbol duration is about 18 dB smaller than during the on-slot. After two symbol durations, it is about 31 dB smaller. Another symbol duration later, the power level is about 50 dB lower. The power level is beneath -50 dB during an off-slot, which is at the noise power level of -80 dBm since the signal has -10 dBm transmit power and the isolation between Tx and Rx on the same USRP is about 15 to 20 dB. In summary, as the signal power is attenuated around 18 dB after one symbol duration, we can assume that at most one symbol is affected by the transient of the RODD signaling (for the tested symbol rate). The off-slots (without the transients) are nicely silent, as required.

C. BER vs. SNR Curves

The BER is calculated only for frames with accurate timing to ensure that timing errors do not affect the results.

Fig. 16 compares the BER curves for the unidirectional experiment, the bidirectional experiment, and the bidirectional simulation[2]. Note that there is a point of Node 1 in bidirectional mode which is zero at 13.21 dB averaged over 10000 runs. It means that the BER is at the level of $\frac{1}{10^4 \times 2560} = 3.91 \times 10^{-8}$ given that the frame length is 2560. The error event has extremely low probability and hence no error is reported in 10000 runs. The curve from the

[2]Only one node's BER curve is plotted since the bidirectional simulation results for both nodes are very close.

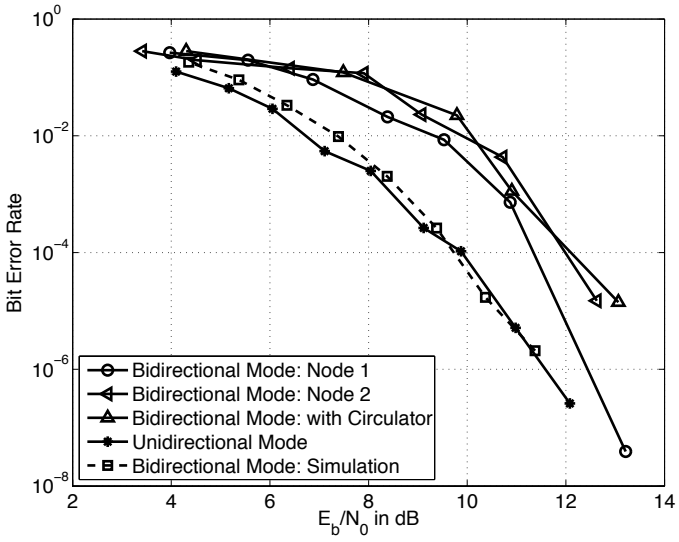

Figure 16: Comparison of BER curves for unidirectional and bidirectional implementation and simulation result.

unidirectional mode is the best since there is no self-interference in this scenario. We observe that the unidirectional mode performs better than the bidirectional mode. This is an expected result, as the self-interference as well as multipath propagation in the bidirectional mode introduce additional challenges for the system. The curves validate that the channel coding designed for RODD system is able to correct the erasures caused by the self-interference. The curve from the setup with circulator has similar performance to that from the two-antenna setup. Hence, both setups work equally well for RODD. The setup with circulator is preferable since it only needs one antenna.

The horizontal gap between the simulation result and the measured curves has mainly two reasons. First, the simulation BER curve is obtained for an ideal AWGN channel, and the AWGN channel differs significantly from the real channel. Second, the relatively small oversampling factor can cause sample timing errors, which results in intersymbol interference.

In summary, we can conclude that the principle of on-off signaling is promising, as the shape of the measured BER curves follows the simulation curve. There is at most a 2 dB difference for most of the experimental measurements in the BER performance due to the practical limitations. Therefore, it can be concluded that the USRP/LabVIEW-based prototype works quite well.

VIII. Concluding Remarks and Future Work

A. Summary

In this paper, we have presented a software-radio implementation of an RODD system to achieve virtual full-duplex operation. We experimentally demonstrate that a pair of nodes can indeed communicate in a full-duplex manner at the frame level. The effects that on-off signaling introduces have been studied and calibrated. The BER performance of unidirectional and bidirectional modes has been measured and compared with the theoretical and simulation results.

In general, it can be concluded that RODD can achieve virtual full duplex in practice. Our results suggest that RODD can indeed overcome the half-duplex constraint as predicted by the theory.

B. Future Work

This is the first proof of concept of RODD. We will test different on-off signaling and coding schemes and compare the link throughput for unidirectional and bidirectional traffic with and without synchronization. We will also test ARQ-type schemes where a receiver can immediately stop the sender once it has acquired enough information for decoding. The extension from two nodes to three or more nodes will be the next big step in our prototype in which an *RODD network* will be created and evaluated.

Acknowledgment

The authors would like to thank Dr. Thomas Fuja for the helpful discussions on the channel coding implementation.

Appendix

Design Space

The parameters of the prototype need to be chosen carefully. There are tradeoffs between different parameters. In the following, we discuss about the choices of some parameters that are not covered in the main body.

A. The Pulse Shaping Filter

First of all, there is some tradeoff between the pulse shaping filter length and the slot length. When the pulse shaping filter is too long, the interference from on-slot to off-slot may become stronger due to the long tail of the filter. We conduct a set of experiments in order to obtain the good choice of the pulse shaping filter. Given fixed slot length, different values for the length of pulse shaping filter affect the BER as shown in Figure 17 below. As seen, the length range with good performance in terms of BER is between 4-8 outside of which the BER suffers from noticeable degradation. Hence, considering both accuracy and efficiency, we choose the length to be 6 which has good performance while not affecting the efficiency.

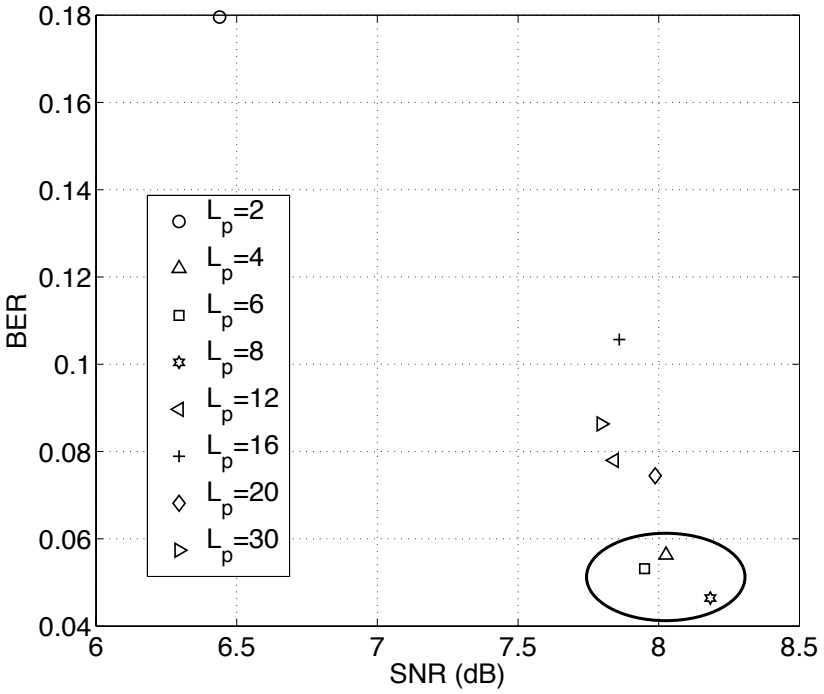

Figure 17: BER vs SNR with different pulse shaping filter length. The Tx attenuation is 16 dB and Rx 31 dB.

Similarly, the rolloff factor of the pulse shaping filter also affects the BER. A good choice needs to be figured out via experiments as well to maker sure the BER is as low as possible. The BER as a function of SNR in dB is plotted for different rolloff factors of the pulse shaping filter. It can be seen that the choice of 0.5 is a good one as it can achieve the lowest BER in Figure 18.

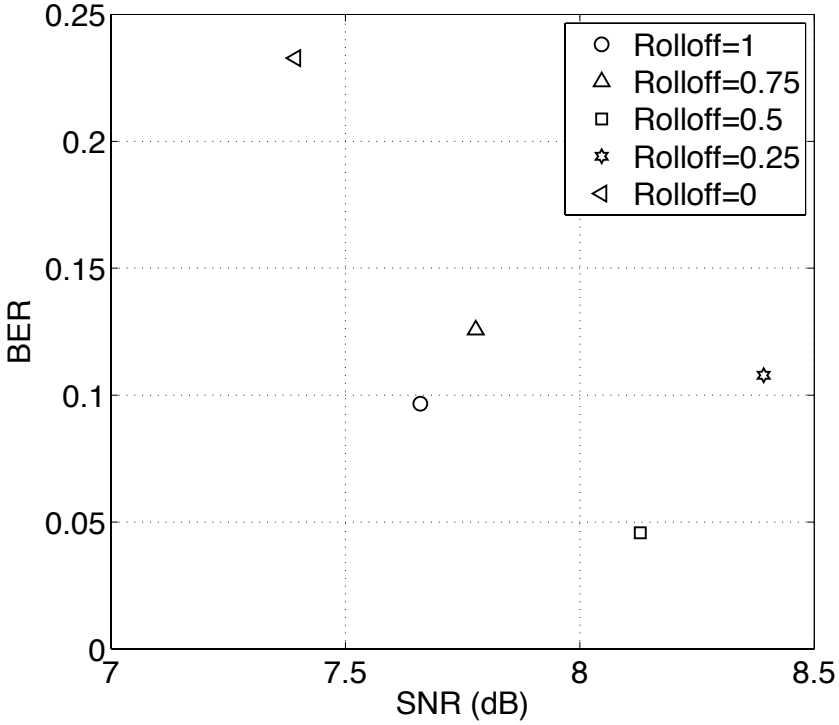

Figure 18: BER vs SNR with different rolloff factors in pulse shaping filter. The pulse shaping filter length is 6. The Tx attenuation is 16 dB and Rx 31 dB.

B. Code Rate vs Duty Cycle

The tradeoff between duty cycle and RS code rate can be analyzed theoretically. Under an AWGN channel, the BER of DBPSK is $P_b = \frac{1}{2}e^{-E_b/N_0}$. Hence, the probability that there is at least one error in one slot with length L and with the first bit as a guard bit is

$$P_{\text{error}} = 1 - (1 - P_b)^{L-1}.$$

The erasures come from two sources: one from self-interference and the other from noise errors since the inner code we designed will label one slot as an erasure when there is any noise error. Given a duty cycle p_D, the erasure rate for a RODD channel with the channel coding scheme presented in our paper is

$$P_{\text{erasure}} = p_D + (1 - p_D)P_{\text{error}}.$$

Hence, the maximal RS code rate achievable is $R_{\max} = 1 - P_{\text{erasure}}$ which is plotted in Figure 19.

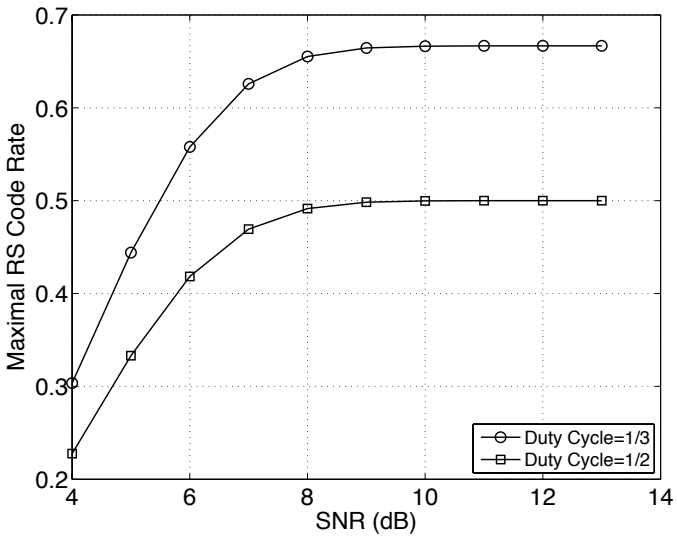

Figure 19: The maximal achievable code rate of RS code vs SNR with different duty cycle under an AWGN channel. The slot length $L = 20$ and the modulation is DBPSK.

As seen, the maximal achievable RS code rate approaches $2/3$ for a duty cycle $p_D = 1/3$ while $1/2$ for $p_D = 1/2$. This maximal achievable code rate is obtained from analysis. When implemented, the erasure rate from the self-interference is a random variable with average as p_D. In order to provide some resilience, we chose code rate $1/2$ when the duty cycle is $1/3$. This code rate works for SNRs greater than 5 dB and is sufficient to correct the erasures from the RODD channel. For SNRs less than 5 dB, it is possible that several on-slots are contaminated by noise errors and hence the RS decoder has to use some of contaminated on-slots to decode which leads to degradation in performance. However, this degradation is reasonable as shown in Figure 9.

C. The Choice of N

When we use the cross-correlation-based timing synchronization and find a value that is greater than the threshold we set, we want to find the maximum peak of the cross correlation. It must be near the first value that exceeds the threshold. Hence, we search its next N values. N can be as large as the slot length but by experiments it is shown that 5 is sufficient to achieve good accuracy while keeping the search efficient. To illustrate the effect that different choices of N have on the timing synchronization, we conduct a set of experiments and plot the result. As illustrated in Figure 20, the timing accuracy does not improve after N is greater than 5 and

hence $N = 5$ is a good choice.

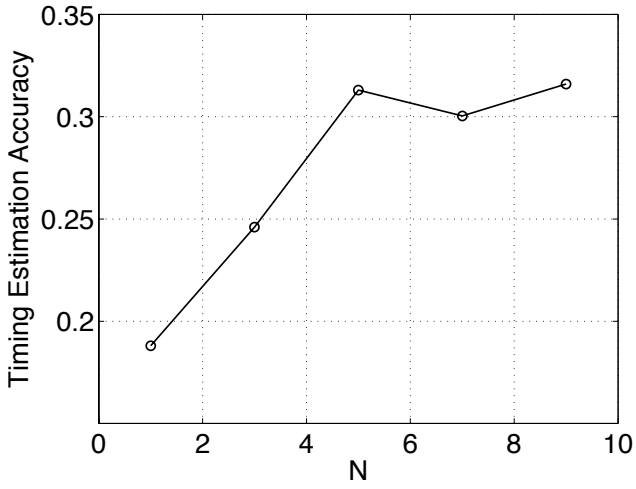

Figure 20: Timing accuracy with different values of N. The Tx attenuation is 16 dB and Rx 31 dB.

E_b/N_0 CALCULATION

In order to be able to measure some values on the BER curve, we first have to know the SNR in the current setup. The relation between E_b/N_0 and SNR is given as follows:

$$\text{SNR} = \frac{E_b}{N_0} \cdot \frac{f_b}{B}, \tag{6}$$

where f_b is the channel data rate, and B is the channel bandwidth. Since binary modulation is used in our experiments, the datarate and the channel bandwidth are the same. Therefore, $E_b/N_0 = \text{SNR}$.

The basic idea to obtain the SNR is to estimate the power of the useful received signal (when only the other node is transmitting) and to estimate the power of a silent off-slot (when no one is transmitting) and divide the results. The different signal types are illustrated in Fig. 21. The interesting slots are the silent off-slot and the one with the desired signal of another node. To avoid that the leakage of the transmitted signal affects the estimated values, 15% of the window size T is ignored at the beginning and the end of a slot for the calculation as illustrated in Fig. 22. T corresponds to the length of one RODD slot in time. This value is reasonable, because as shown in Section VII-B, the side lobes are decreased by more than 30 dB after two symbols, which is 10% of a slot with size 20.

As the measurement setup is static, we assume that the E_b/N_0 stays nearly the same within one frame. The E_b/N_0 is calculated once for each frame. To increase the accuracy of E_b/N_0, all the non-erased slots with wanted received signal and all the silent off-slots during the preamble of one on-off frame are used to the E_b/N_0 calculation.

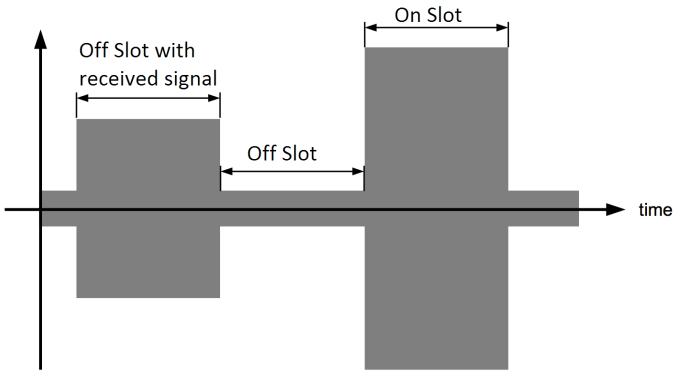

Figure 21: Illustration of RODD signaling with off-slot that contains wanted signal and noise, respectively, as well as an on-slot with self-interference.

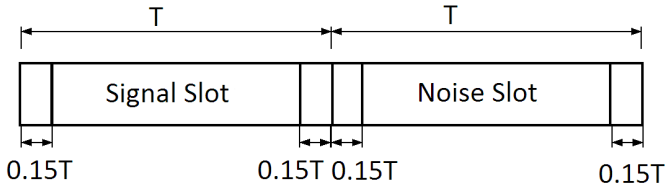

Figure 22: Illustration of signal structure for the SNR calculation.

The procedure leads not exactly to the SNR ($\frac{S}{N}$), rather to $\frac{S+N}{N} = \frac{S}{N} + 1$. Therefore the value is reduced by 1 before conversion to dB. To achieve different E_b/N_0 values, a combination of some factors is used. First of all the transmit/receive power gains can be set in software. For the transmitter the value can be set from 0 dB to 31 dB. The maximum output power using frequencies from 50 MHz to 1.2 GHz (we use 915 MHz for the measurements) is 17 dBm to 20 dBm (50 mW to 100 mW) [5]. The receiver's gain range is from 0 dB to 31.5 dB, and its maximum input power is 0 dBm (1 mW) [5]. The measurements in our experiments are made with all power gains set to 0 dB, which is the minimal gain for both transmitter and receiver in order to achieve the desired SNR range. Thus the output power at the transmitter is at most

-10 dBm (0.1 mW). Moreover, attenuators are used to further decrease the SNR to the range of interest in the experiments.

Next, for the unidirectional benchmark an RF cable is used to connect the transmitter of one USRP with the receiver of the other USRP. To achieve different E_b/N_0 we attached different amounts of attenuators to the cable. The settings are summarized in Tables II and III. The unidirectional mode is a more controlled measurement setup than the bidirectional mode. As an RF cable is used between the two USRPs, the SNR does not depend on the actual setup of the antennas or the position of the USRPs. Thus the measurements for different SNR values are not affected by changes in the placement of the USRPs. In contrast, the bidirectional mode is quite sensitive to such changes. The first column in Table III is the hardware attenuation added to the transmitter side between the Tx antenna and the RF font end and the second column for the receiver side. The resulting SNRs at both nodes with standard deviation are summarized in the third and fourth columns.

attenuation (dB)	resulting E_b/N_0 (dB)
71	4.10 ± 0.52
70	5.17 ± 0.53
69	6.05 ± 0.53
68	7.11 ± 0.55
67	8.04 ± 0.55
66	9.12 ± 0.57
65	9.87 ± 0.57
64	10.98 ± 0.58
63	12.08 ± 0.59

Table II: Settings for different E_b/N_0 values for the BER measurement in unidirectional mode.

REFERENCES

[1] A. Sahai, G. Patel, and A. Sabharwal, "Pushing the limits of full-duplex: Design and real-time implementation," *Rice tech report*, 2011, online: http://arxiv.org/abs/1107.0607.

[2] D. Guo and L. Zhang, "Virtual full-duplex wireless communication via rapid on-off-division duplex," in *2010 48th Annual Allerton Conference on Communication, Control, and Computing (Allerton)*, 2010, pp. 412–419.

[3] L. Zhang and D. Guo, "Virtual full duplex wireless broadcasting via compressed sensing," *IEEE/ACM Trans. on Networking*, vol. 22, pp. 1659–1671, October 2014.

attenuation at Tx (dB)	attenuation at Rx (dB)	resulting E_b/N_0 (dB) at Node 1	resulting E_b/N_0 (dB) at Node 2
18	34	3.92 ± 0.61	3.68 ± 0.62
17	34	5.13 ± 0.61	4.40 ± 0.66
18	31	6.74 ± 0.65	6.09 ± 0.66
17	31	8.11 ± 0.65	7.90 ± 0.65
15	31	9.53 ± 0.66	9.08 ± 0.65
13	31	10.87 ± 0.66	10.72 ± 0.67
12	31	13.21 ± 0.66	12.63 ± 0.68

Table III: Settings for different E_b/N_0 values for the BER measurement in bidirectional mode.

attenuation at Tx (dB)	attenuation at Rx (dB)	resulting E_b/N_0 (dB) at Node with Circulator
18	31	4.30 ± 0.57
16	31	7.49 ± 0.63
14	31	9.79 ± 0.65
12	31	10.90 ± 0.66
10	31	13.06 ± 0.70

Table IV: Settings for different E_b/N_0 values for the BER measurement in bidirectional mode from Fig. 4c.

[4] ——, "Neighbor discovery in wireless networks using compressed sensing with Reed-Muller codes," in *2011 International Symposium on Modeling and Optimization in Mobile, Ad Hoc and Wireless Networks (WiOpt)*, 2011, pp. 154–160.

[5] National Instruments Cooperation, "Device specifications NI USRP 2920 50 MHz to 2.2 GHz Tunable RF Transceiver," National Instruments Cooperation, Online at http://www.ni.com/pdf/manuals/375839a.pdf.

[6] R. E. Ziemer and W. H. Tranter, *Principles of Communications*, 6th ed. Wiley Publishing, 2008.

[7] H. O. Peterson, J. B. Attwood, H. E. Goldstine, G. E. Hansell, and R. E. Schock, "Observations and comparisons on radio telegraph signaling by frequency shift and on-off keying," *RCA Review*, vol. 12, pp. 11–32, Mar. 1946.

[8] M. Z. Win and R. A. Scholtz, "Ultra-wide bandwidth time-hopping spread-spectrum impulse radio for wireless multiple-access communications," *IEEE Transactions on Communications*, vol. 48, pp. 679–691, 2000.

[9] G. R. Kenworthy, "Self-cancelling full-duplex RF communication system," in *US Patent 5,691,978*, 1997.

[10] S. Chen, M. A. Beach, and J. P. McGeehan, "Division-free duplex for wireless applications," *Electronics Letters*, vol. 34, no. 2, pp. 147–148, 1998.

[11] J. I. Choi, M. Jain, K. Srinivasan, P. Levis, and S. Katti, "Achieving single channel, full duplex wireless communication," in *Proceedings of the 16th Annual International Conference on Mobile Computing and Networking (MobiCom'10)*, New York, NY, USA, 2010, pp. 1–12. [Online]. Available: http://doi.acm.org/10.1145/1859995.1859997

[12] M. Duarte and A. Sabharwal, "Full-duplex wireless communications using off-the-shelf radios: Feasibility and first results," in *2010 Conference Record of the Forty Fourth Asilomar Conference on Signals, Systems and Computers (ASILOMAR)*, 2010, pp. 1558–1562.

[13] M. Jain, J. I. Choi, T. Kim, D. Bharadia, S. Seth, K. Srinivasan, P. Levis, S. Katti, and P. Sinha, "Practical, real-time,

full duplex wireless," in *Proceedings of the 17th Annual International Conference on Mobile Computing and Networking (MobiCom'11)*, New York, NY, USA, 2011, pp. 301–312. [Online]. Available: http://doi.acm.org/10.1145/2030613.2030647

[14] D. Bharadia, E. McMilin, and S. Katti, "Full duplex radios," *SIGCOMM Comput. Commun. Rev.*, vol. 43, no. 4, pp. 375–386, Aug. 2013. [Online]. Available: http://doi.acm.org/10.1145/2534169.2486033

[15] Z. Tong and M. Haenggi, "Throughput analysis for wireless networks with full-duplex radios," in *2015 IEEE Wireless Communications and Networking Conference (WCNC'15)*, New Orleans, LA, USA, March 2015.

[16] ——, "Throughput analysis for full-duplex wireless networks with imperfect self-interference cancellation," *IEEE Transactions on Communications*, 2015, submitted, available online at http://arxiv.org/abs/1502.07404.

[17] A. K. Khandani, "Two-way (true full-duplex) wireless," in *2013 13th Canadian Workshop on Information Theory (CWIT)*, June 2013, pp. 33–38.

[18] E. Aryafar, M. A. Khojastepour, K. Sundaresan, S. Rangarajan, and M. Chiang, "MIDU: Enabling MIMO full duplex," in *Proceedings of the 18th Annual International Conference on Mobile Computing and Networking (Mobicom'12)*, New York, NY, USA, 2012, pp. 257–268. [Online]. Available: http://doi.acm.org/10.1145/2348543.2348576

[19] B. Chen, Y. Yenamandra, and K. Srinivasan, "Flexradio: Fully flexible radios," *Technical Report*, 2013, online: http://web.cse.ohio-state.edu/~kannan/cosyne/nsdi14-anyduplex.pdf.

[20] T. Yucek and H. Arslan, "A survey of spectrum sensing algorithms for cognitive radio applications," *Communications Surveys & Tutorials, IEEE*, vol. 11, no. 1, pp. 116–130, 2009.

[21] M. E. Knox, "Single antenna full duplex communications using a common carrier," in *2012 IEEE 13th Annual Wireless and Microwave Technology Conference (WAMICON)*, 2012, pp. 1–6.

[22] Fairview Microwave, "SMA Circulator with 19 dB isolation from 800 MHz to 960 MHz," Fairview Microwave, Online at http://www.fairviewmicrowave.com/images/productPDF/SFC8096.pdf.

[23] J. Heiskala and J. Terry, *OFDM Wireless LANs: A Theoretical and Practical Guide*. Sams Publishing, 2002.

[24] L. Rizzo, "Effective erasure codes for reliable computer communication protocols," *SIGCOMM Comput. Commun. Rev.*, vol. 27, no. 2, pp. 24–36, Apr. 1997. [Online]. Available: http://doi.acm.org/10.1145/263876.263881

[25] S. Lin and D. J. Costello, *Error Control Coding, Second Edition*. Upper Saddle River, NJ, USA: Prentice-Hall, Inc., 2004.

[26] J. W. Byers, M. Luby, M. Mitzenmacher, and A. Rege, "A digital fountain approach to reliable distribution of bulk data," *SIGCOMM Comput. Commun. Rev.*, vol. 28, no. 4, pp. 56–67, Oct. 1998. [Online]. Available: http://doi.acm.org/10.1145/285243.285258

[27] E. Paolini, G. Liva, and M. Chiani, "High Throughput Random Access via Codes on Graphs: Coded Slotted ALOHA," in *2011 IEEE International Conference on Communications (ICC)*, June 2011, pp. 1–6.

[28] ——, "Coded slotted ALOHA: A graph-based method for uncoordinated multiple access," *CoRR*, vol. abs/1401.1626, 2014. [Online]. Available: http://arxiv.org/abs/1401.1626

[29] S. Vanka, S. Srinivasa, Z. Gong, P. Vizi, K. Stamatiou, and M. Haenggi, "Superposition Coding Strategies: Design and Experimental Evaluation," *IEEE Transactions on Wireless Communications*, vol. 11, no. 7, pp. 2628–2639, Jul. 2012.